ISSN 1063-7761, Journal of Experimental and Theoretical Physics, 2015, Vol. 120, No. 1, pp. 103–109. © Pleiades Publishing, Inc., 2015.
Original Russian Text © V.S. Zhandun, N.G. Zamkova, V.I. Zinenko, 2015, published in Zhurnal Eksperimental'noi i Teoreticheskoi Fiziki, 2015, Vol. 147, No. 1, pp. 119–126.

ORDER, DISORDER, AND PHASE TRANSITION IN CONDENSED SYSTEM

Effect of an Eu^{3+} Impurity on the Antiferrodistortion and Ferroelectric Instabilities in an $EuTiO_3$ Bulk Crystal and Thin Films

V. S. Zhandun*, N. G. Zamkova, and V. I. Zinenko

Kirensky Institute of Physics, Siberian Branch, Russian Academy of Sciences, Krasnoyarsk, 660036 Russia

**e-mail: jvc@iph.krasn.ru*

Received May 30, 2014

Abstract—The existence of an antiferrodistortion transition in $EuTiO_3$ is disputable, and this question needs to be answered. One of the possible causes is the presence of an Eu^{3+} impurity in a sample. A nonempirical polarizable ion model is used to study the effect of a trivalent Eu^{3+} ion impurity on the antiferrodistortion and ferroelectric instabilities of an $EuTiO_3$ crystal in the bulk and the thin-film states. Lattice dynamics calculation shows that a bulk impurity-free $EuTiO_3$ crystal has no unstable modes throughout the entire phase space volume. The addition of an Eu^{3+} impurity leads to a significant softening of the rotational mode, the distortion in which makes tetragonal phase $I4/mcm$ (which is experimentally observed) energetically favorable. In going from the bulk crystal to the thin film, the vibration spectrum of the impurity-free film has unstable antiferrodistortion and rotational modes. The addition of an Eu^{3+} impurity enhances the antiferrodistortion instability, which fully or partly suppresses ferroelectricity.

DOI: 10.1134/S1063776115010070

1. INTRODUCTION

The $EuTiO_3$ oxide solidifies into a perovskite structure with space group $Pm3m$ and unit cell parameter $a = 3.9$ Å, which is very close to the lattice parameter of $SrTiO_3$ [1]. $EuTiO_3$ was studied in numerous experimental and theoretical works, and interest in this compound has been recently quickened and is caused by the possibility of coexistent magnetic and electric order parameters. At $T_N = 5.3$ K, $EuTiO_3$ undergoes an antiferromagnetic phase transition [2, 3]. A ferroelectric phase transition in a bulk $EuTiO_3$ crystal is not detected up to the liquid-helium temperature. The ab-initio calculations of the $EuTiO_3$ lattice (perovskite structure) dynamics also do not reveal a ferroelectric instability in the crystal lattice, and the polar mode turns out to be harder than in $SrTiO_3$ [4]. Nevertheless, by analogy with $SrTiO_3$, the authors of [5, 6] attribute $EuTiO_3$ to quantum paraelectrics. The calculation [7] of the properties of thin $EuTiO_3$ films showed that a ferroelectric instability appears in them when tensile stresses are applied to the films [8]. As for the structural antiferrodistortion transition in $EuTiO_3$, conflicting data on this subject are available, as on the transition in $SrTiO_3$ and the transition related to the rotation of the TiO_6 ($a^0a^0c^-$ in the designations in [9]) oxygen octahedron. Using ab initio VASP calculations, the authors of [4] showed that the polar modes in the phonon spectrum of this compound are stable and that additional strong instabilities also exist at boundary points R and M in the Brillouin zone. The energies of possible phases $I4/mcm$, $Imma$, and $R\bar{3}c$, which are associated with antiferrodistortion distortions $a^0a^0c^-$, $a^0b^-b^-$, and $a^-a^-a^-$ of the cubic phase, turned out to be close to each other. Using ab initio calculations, the authors of [10] concluded that the antiferrodistortion instability in an $EuTiO_3$ is caused by the hybridization of the f electrons of Eu and the d electrons of Ti. The effect of Hubbard U on the stability of the rotational mode was studied, and an increase of U_{Eu} (f electrons of Eu become more localized) was found to stabilize the antiferrodistortion mode. Such a transition from the cubic $Pm3m$ ($z = 1$) phase into the tetragonal $I4/mcm$ phase ($z = 2$) was experimentally detected [11–14], and the transition temperatures differ substantially in different experiments (from 162 K [12] to 282 K [11]). On the other hand, the authors of [15] studied the temperature dependence of the specific heat of $EuTiO_3$ and did not detect anomalies related to structural transitions down to the liquid-helium temperature. They explained this behavior by the fact that, at the transition temperatures detected in other experiments, oxygen octahedra undergo local antiferrodistortion deformation and the crystal structure remains cubic as a whole. Therefore, they concluded that an internal disorder is important for an analysis of the antiferrodistortion transition in $EuTiO_3$.

When studying $EuTiO_3$ by various techniques, the authors of [16] detected a phase transition into the tet-

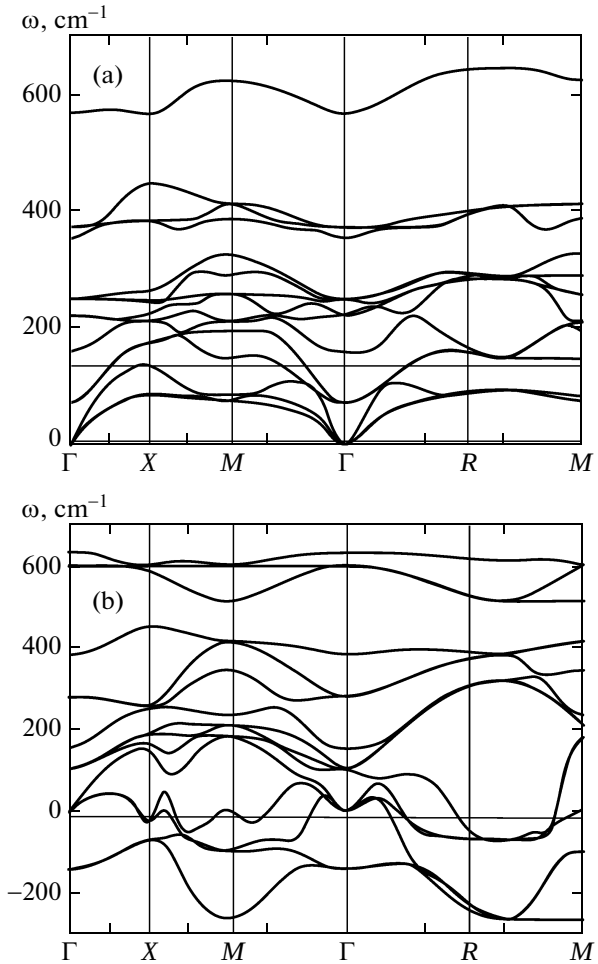

Fig. 1. Phonon spectrum of bulk (a) $Eu^{2+}Ti^{4+}O_3$ and (b) $Eu^{3+}Ti^{3+}O_3$ crystals. Imaginary frequencies are negative.

ragonal $I4/mcm$ phase, which is related to antiferrodistortion lattice deformation, at $T = 300$ K in some cases and found no tangential lattice distortions down to $T = 100$ K in other cases. Based on these data, they assumed that the different antiferrodistortion transition temperatures detected experimentally and the existence of a structural transition in $EuTiO_3$ can be related to the presence of either a trivalent Eu^{3+} ion impurity or oxygen vacancies in samples. The authors of [5, 17] also noted that, apart from the divalent Eu^{2+} ion, the trivalent Eu^{3+} ion can also exist in $EuTiO_3$ during its growth.

Therefore, the purpose of this work was to study the effect of trivalent Eu^{3+} ion impurities in an $Eu^{2+}Ti^{4+}O_3$ crystal on the ferroelectric and antiferrodistortion instabilities in a bulk crystal and thin crystal films.

2. CALCULATION PROCEDURE

The calculations were performed in terms of a nonempirical polarizable ion model using the density functional theory in the local density approximation [18]. The effective charges were calculated according to [19]. The equilibrium lattice parameter was obtained by minimizing the total crystal energy at various trivalent Eu^{3+} impurity concentrations. The calculation of thin films was carried out in periodic layer geometry: the films were considered to consist of periodic alternating EuO and TiO_2 atomic planes. To isolate the layers from each other, we introduced a vacuum layer four perovskite lattice parameters thick between them. We used the virtual crystal approximation to calculate the lattice dynamics and the energetics of $EuTiO_3$ crystals doped with Eu^{3+} [20].

3. RESULTS AND DISCUSSION

3.1. Bulk Crystal

The lattice dynamics of an $EuTiO_3$ crystal having a perovskite structure with space group $Pm3m$ was calculated using the minimum lattice parameter, which turned out to be $a = 3.82$ Å for an $Eu^{2+}Ti^{4+}O_3$ crystal (which is smaller than the experimental parameter by approximately 2%) and $a = 3.87$ Å for a hypothetical $Eu^{3+}Ti^{3+}O_3$ crystal.

Figure 1 shows the phonon spectra of the crystals in the symmetric directions of the Brillouin zone, and Table 1 gives the high-frequency permittivity and the effective Born charges for the compounds with di- and trivalent europium ions.

As is seen in Fig. 1, the phonon spectrum of $Eu^{2+}Ti^{4+}O_3$ has no unstable modes, and the vibration frequencies of "potential" unstable modes have rather high values, about 100 cm^{-1}. The latter modes are represented by the transverse polar Γ_{15} ($q = 0$) mode and the modes related to the "rotation" of the oxygen octahedron, namely, R_{25} ($q = 1/2(b_1 + b_2 + b_3)$) and M_3 ($q = 1/2(b_1 + b_2)$), where b_α is the reciprocal lattice vector. These results for $Eu^{2+}Ti^{4+}O_3$ contradict the calculation results in [4], where unstable modes R_{25} and M_3 were detected (see Introduction). We repeated the calculation of [4] using the VASP software package

Table 1. Effective charges Z^* (in units of e) and high-frequency permittivity ε for a bulk $Eu^{2+}Ti^{4+}O_3$ crystal and a hypothetical $Eu^{3+}Ti^{3+}O_3$ crystal

	Z^*(Eu)	Z^*(Ti)	$Z^*(O_\perp)$	$Z^*(O_\parallel)$	ε
$Eu^{2+}Ti^{4+}O_3$	2.68	5.70	–5.0	–1.71	4.51
$Eu^{3+}Ti^{3+}O_3$	3.78	4.15	–2.2	–2.81	5.08

and two lattice parameters, namely, the equilibrium and experimental parameters. Note that the calculation in [4] was performed using the experimental lattice parameter, which is smaller than the equilibrium parameter obtained in our calculation by 1%. Using the equilibrium unit cell parameter (a = 3.94 Å), we obtained unstable modes R_{25} and M_3 ($\omega \approx 80$ cm^{-1}), the eigenvectors of which correspond to the rotation of the oxygen octahedron.

As is seen from Fig. 1b, the hypothetical $Eu^{3+}Ti^{3+}O_3$ compound, where Eu^{3+} fully substitutes for Eu^{2+} and Ti^{3+} substitutes for Ti^{4+}, has high unstable vibration modes, which occupy the entire reciprocal space volume. The softest modes with a frequency of about 250 cm^{-1} correspond to the instability of the lattice with respect to the rotation of the $Ti^{3+}O_6$ octahedron.

The physical cause of this instability in the $Eu^{3+}Ti^{3+}O_3$ compound can be illustrated by the example of triply degenerate mode R_{25}. The squared frequency of mode R_{25} for a perovskite structure can be analytically expressed in terms of dynamic matrix elements as follows:

$$\omega_i^2 = e_i - g_i, \quad i = 1, 2, 3, \tag{1}$$

where $e_1 = d^{yy}_{O_1O_1}$ are the diagonal and $g_1 = d^{xy}_{O_1O_2}$ are the off-diagonal elements of the dynamic matrix (DM), and e_2, e_3 and g_2, g_3 can be obtained by the cyclic permutation $O_1(0.0, 0.5, 0.5) \longrightarrow O_2(0.5, 0.0, 0.5) \longrightarrow O_3(0.5, 0.5, 0.0)$ and $y \longrightarrow z \longrightarrow x$. Table 2 gives the calculated contributions to DM elements e_1 and g_1 for $Eu^{3+}Ti^{3+}O_3$ and $Eu^{2+}Ti^{4+}O_3$. In both cases, the main contributions to $\omega^2_{R_{25}}$ are made by Coulomb long- and short-range contributions, and the competition between them determines the sign of $\omega^2_{R_{25}}$. The difference between the short-range contributions is insignificant and appears because of the difference between the lattice parameters of $Eu^{3+}Ti^{3+}O_3$ and $Eu^{2+}Ti^{4+}O_3$, whereas the long-range Coulomb contributions to the diagonal elements of DM in $Eu^{3+}Ti^{3+}O_3$ are almost half the contributions in $Eu^{2+}Ti^{4+}O_3$. The Coulomb contribution to $\omega^2_{R_{25}}$ is positive for $Eu^{2+}Ti^{4+}O_3$ and exceeds the negative contribution of the short-range term in DM, whereas both contributions in $Eu^{3+}Ti^{3+}O_3$ are negative, which results in a negative value of $\omega^2_{R_{25}}$ and, hence, an antiferrodistortion instability.

The following three versions of charge compensation to ensure electroneutrality are possible when a trivalent Eu^{3+} ion impurity is introduced: compensation occurs via vacancy formation at site A in the perovskite structure occupied by an Eu^{2+} ion ($Eu^{2+}_{1-x}Eu^{3+}_{2x/3}\square_{x/3}Ti^{4+}O_3$); vacancy appears at site B occupied by a Ti^{4+} ion ($Eu^{2+}_{1-x}Eu^{3+}_{x}Ti^{4+}_{1-x/4}\square_{x/4}O_3$), where $\square$ is a vacancy; and finally, Ti^{3+} ions substitute for some Ti^{4+} ions ($Eu^{2+}_{1-x}Eu^{3+}_{x}Ti^{4+}_{1-x}Ti^{3+}_{x}O_3$).

Table 2. Contributions to the dynamic matrix (10^{-4} au) of $EuTiO_3$ in a perovskite structure

	$Eu^{2+}Ti^{4+}O_3$			$Eu^{3+}Ti^{3+}O_3$		
	e	g	$\omega^2_{R_{25}}$	e	g	$\omega^2_{R_{25}}$
Short-range contribution	−4	9	−13	−4	2	−12
Coulomb contribution	71	48	23	37	46	−9

We calculated the minimum lattice parameter for each version of charge compensation and complete substitution of trivalent for divalent europium and found that the formation of a vacancy at the Eu^{2+} and Ti^{4+} sites decreases the equilibrium lattice parameter by 0.05 Å and the substitution of Ti^{3+} for Ti^{4+} increases it by 0.05 Å. The calculation during a change in the Eu^{3+} impurity concentration was calculated using the lattice parameters computed by Vegard's law [21].

The lattice dynamics calculation showed that the modes related to the rotation of the oxygen octahedron and the polar mode are softened during the charge compensation via the formation of a vacancy at site A of the perovskite structure when Eu^{3+} gradually substitutes for divalent Eu^{2+}. Nevertheless, these modes remain hard up to high concentrations (Fig. 2). The situation changes when a vacancy forms at site B of the perovskite structure or when Ti^{3+} substitutes for Ti^{4+}. It is seen in Fig. 2 that, as the Eu^{3+} ion concentration increases, the antiferrodistortion mode also softens and becomes soft at an Eu^{3+} concentration x = 0.35 (substitution of Ti^{3+} for Ti^{4+}) and x = 0.45 (vacancy at the Ti^{4+} site).

When a vacancy forms at the site of the Ti^{4+} ion during the introduction of an Eu^{3+} impurity, we found that the distortion of the crystal in the eigenvector of the antiferrodistortion mode at a trivalent ion impurity concentration x = 0.45 makes the tetragonal phase favorable. This phase is associated with rotation $a^0a^0c^-$ (space group $I4/mcm$) and is experimentally observed in the $EuTiO_3$ compounds where a structural transition exists. A further increase in the Eu^{3+} concentration leads to the fact that, first, rotation $a^0b^-b^-$ and, then, rotations $a^-a^-a^-$ and $a^-a^-c^+$ become favorable. Table 3 gives the energies of these most favorable low-symmetry phases at several Eu^{3+} concentrations and the angles of oxygen octahedron rotation that correspond to the energy minimum in these phases. As is seen from Table 3, the energies of the phases with distortions $a^0a^0c^-$, $a^0b^-b^-$, $a^-a^-a^-$, and $a^-a^-c^+$ are close at the given Eu^{3+} concentrations. It should be noted that the authors of [4], where the calculation was per-

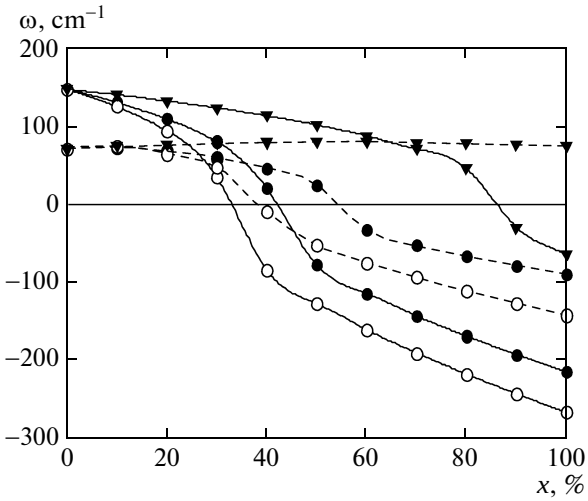

Fig. 2. Antiferrodistortion and ferroelectric mode frequencies vs. the Eu^{3+} impurity concentration in a bulk $EuTiO_3$ crystal for various versions of charge compensation. (triangles) Vacancy at the Eu^{2+} site, (filled symbols) vacancy at the Ti^{4+} site, (open symbols) substitution of Ti^{3+} for Ti^{4+}. (dashed lines) Ferroelectric and (solid lines) antiferrodistortion modes. Imaginary frequencies are negative.

formed with the VASP software package, also obtained close energies of the phases related to rotations $a^0a^0c^-$, $a^0b^-b^-$, and $a^-a^-a^-$. In the case of charge compensation with the substitution of Ti^{3+} for Ti^{4+}, the energies of all the phases noted above are also close to each other, and the phases with rotations $a^-a^-a^-$ and $a^-a^-c^+$ are most favorable at various concentrations.

As for the ferroelectric instability, it is seen from Fig. 2 that the polar mode frequency squared becomes negative at a higher Eu^{3+} impurity concentration, which makes a ferroelectric phase transition unlikely (since the antiferrodistortion transition is known to suppress the ferroelectric instability).

3.2. Thin Films

The calculation procedure described above was applied to computing the lattice dynamics and the energies of the low-symmetry phases in thin $EuTiO_3$ films of the following thicknesses: two perovskite unit cells (5 monoatomic layers) and eight perovskite unit cells (17 monoatomic layers). In contrast to the bulk crystal, the vibration spectrum of an $Eu^{2+}Ti^{4+}O_3$ film has antiferrodistortion instabilities at point M of the Brillouin zone and a ferroelectric instability at the center of the Brillouin zone for the films with both thicknesses. The Eu ions located on the film surface mainly undergo displacement in the eigenvector of the ferroelectric mode, and the displacement of the atoms in the film volume is small and decreases toward the center of the film, which is most pronounced at a film thickness of 17 monolayers. As for the eigenvector of the antiferrodistortion modes, there are two unstable antiferrodistortion modes with close frequencies in the five-layer film; these modes are related to the rotations of two oxygen octahedra toward one side ($a^0a^0c^-$ in the designations of Glazer) and toward different sides ($a^0a^0c^+$ in the designations of Glazer). As the film thickness increases, the number of antiferrodistortion modes at point M of the two-dimensional Brillouin zone increases, since some points in the cubic Brillouin zone in the M–R direction pass to point M of the two-dimensional zone when lattice parameter c of the perovskite structure increases severalfold and since the perovskite structure has an almost dispersion-free vibration branch the eigenvectors of which correspond to the rotation of the oxygen octahedron for any point in the M–R direction. The 17-layer film has six such unstable modes. The squared frequencies of these unstable rotational modes are close to each other at point M. Two modes of them, which are related to rotations $a^0a^0c^-$ and $a^0a^0c^+$ of oxygen octahedra, are softest, as in the case of the five-layer film. The oxygen atoms located near the surface undergo the maximum displacement during rotation.

When a trivalent Eu^{3+} ion impurity is added, the antiferrodistortion and ferroelectric modes are significantly softened irrespective of the type of charge compensation (see Fig. 3).

The calculation of the energies of the phases distorted in the eigenvectors of the antiferrodistortion

Table 3. Difference between the energies E (meV) of the cubic and distorted antiferrodistortion phases and the angle of oxygen octahedron rotation θ in a bulk $EuTiO_3$ crystal vs. impurity Eu^{3+} concentration x

x	$a^0a^0c^-$	θ	$a^0b^-b^-$	θ	$a^-a^-a^-$	θ	$a^-a^-c^+$	θ
				$Eu^{2+}_{1-x}Eu^{3+}_xTi^{4+}_{1-x/4}\square_{x/4}O_3$				
0.45	−8.4	5.1°	−7.0	5.8°	−7.8	5.0°	−7.6	5.0°
0.5	−19.4	6.1°	−20.6	6.8°	−19.7	7.2°	−20.2	7.2°
0.6	−62.6	8.6°	−63.4	8.6°	−63.9	9.4°	−66.7	9.4°
				$Eu^{2+}_{1-x}Eu^{3+}_xTi^{4+}_{1-x}Ti^{3+}_xO_3$				
0.35	−10.2	5.7°	−10.8	5.3°	−11.4	5.5°	−11.4	6.0°
0.4	−31.3	7.3°	−32.9	7.6°	−34.8	7.6°	−35.2	8.2°

and ferroelectric modes showed that both types of distortion in these modes are favorable. Table 4 gives the energies of the ferroelectric and antiferrodistortion phases along with the angles of rotation of a near-surface oxygen octahedron for three Eu^{3+} concentrations, $x = 0$, 0.2, and 0.5. In this case, the *Pmm*2 ferroelectric phase is more favorable than the antiferrodistortion *P*4/*mbm* phase in $Eu^{2+}Ti^{4+}O_3$ and $Eu^{2+}_{0.8}Eu^{3+}_{0.133}\square_{(x/3)_{0.066}}Ti^{4+}O_3$. However, as the Eu^{3+} concentration increases, the antiferrodistortion phase becomes more favorable for all versions of charge compensation. The substitution of trivalent titanium ions for tetravalent ions ($Eu^{2+}_{1-x}Eu^{3+}_{x}Ti^{4+}_{1-x}Ti^{3+}_{x}O_3$) is the most favorable energy version of charge compensation, as in the case of the bulk crystal (see Table 4).

The ferroelectric instability is retained in the antiferrodistortion phase in the five-layer film after the rotation of the oxygen octahedron at the center of the Brillouin zone. The phase distorted in the eigenvector of the antiferrodistortion mode and, then, the eigenvector of the soft polar mode has polar symmetry group *Pm*. In the case of the 17-layer film, the rotation of the oxygen octahedron leads to the disappearance of the ferroelectric instability in the antiferrodistortion phase during the formation of a vacancy at the Ti^{4+} or the Eu^{3+} site.

The spontaneous polarization in the polar *Pmm*2 and *Pm* phases for all films with various types of charge compensation during the introduction of an Eu^{3+} impurity was calculated by the formula

$$P_\alpha = \Sigma_{k,\beta} Z^*_{k,\alpha\beta} \Delta u_{k,\beta},$$

where $Z^*_{k,\alpha\beta}$ are the effective Born charges in the nonpolar phase and $\Delta u_{k,\beta}$ is the difference between the atom coordinates in the nonpolar and polar phases. The calculated values of spontaneous polarization are given in Table 5.

As is seen from Table 5, the polarization in the thick 17-layer films is lower than in the five-layer films and is absent for certain versions of charge compensation when an impurity is added. This behavior can be related to the fact that, as the number of monoatomic layers increases, the properties of a thin film tend toward the properties of the bulk crystal, where ferroelectricity is absent at any Eu^{3+} impurity concentrations. As would be expected, an increase in the Eu^{3+} impurity concentration enhances both the octahedron rotation–related distortions and the polar distortions. However, the antiferrodistortion deformation partly or completely suppresses the ferroelectric lattice instability, which leads to lower polarization in a thin film with an Eu^{3+} impurity as compared to the impurity-free compound.

4. CONCLUSIONS

The main results of this work are as follows.

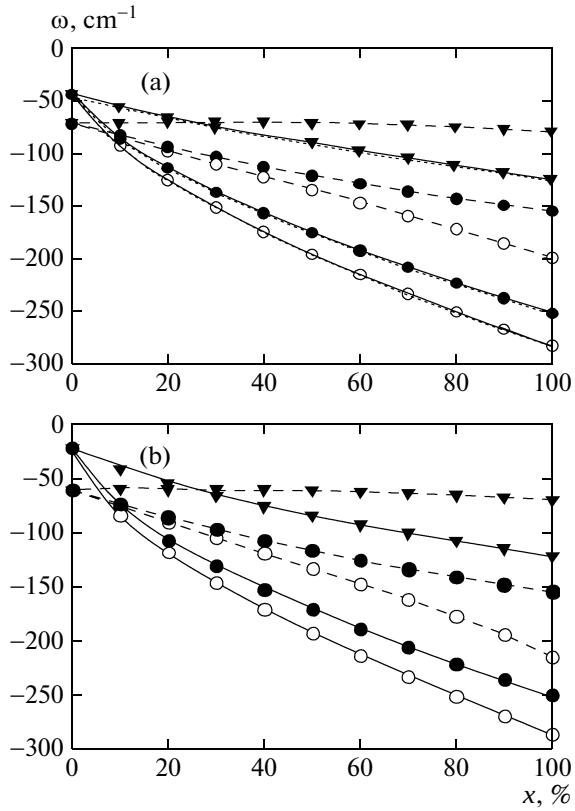

Fig. 3. Ferroelectric and antiferrodistortion mode frequencies in thin $EuTiO_3$ films vs. the impurity Eu^{3+} concentration for various versions of charge compensation: (a) five-layer film and (b) 17-layer film. (triangles) Vacancy at the Eu^{2+} site, (filled symbols) vacancy at the Ti^{4+} site, (open symbols) substitution of Ti^{3+} for Ti^{4+}. (dashed lines) Ferroelectric and (solid lines) antiferrodistortion modes. Imaginary frequencies are negative.

Using a nonempirical polarizable ion model, we studied the properties of $Eu^{2+}Ti^{4+}O_3$ with an Eu^{3+} impurity in the bulk and the thin-film states and found that the phonon spectrum of bulk $Eu^{2+}Ti^{4+}O_3$ has no unstable modes. This result is in conflict with the results of the ab initio calculation of the lattice dynamics with the VASP software package [4] and is supported by the results of the experimental studies of specific heat [13] and XRD [14], where no anomalies indicating a structural phase transition in $EuTiO_3$ samples were detected down to low temperatures. However, the calculation demonstrates that the unstable modes in a hypothetical $Eu^{3+}Ti^{3+}O_3$ crystal occupy the entire phase space volume. The partial substitution of the trivalent for the divalent ion was studied in the virtual crystal approximation. Although this approximation is rather rough, the results of calculating the impurity-containing compound have a qualitative character and are thought to be interesting.

First, the addition of an Eu^{3+} ion impurity instead of Eu^{2+} results in the appearance and enhancement of the antiferrodistortion instability in the bulk crystal.

Table 4. Difference between the energies E (meV) of the cubic and distorted ferroelectric and antiferrodistortion phases and the angle of oxygen octahedron rotation θ in thin $EuTiO_3$ films vs. impurity Eu^{3+} concentration x

x	5 monolayers			17 monolayers		
	E_s	E_{af}	θ	E_s	E_{af}	θ
0	−18.0	−2.3	3.2°	−2.2	−0.1	1.2°
$Eu^{2+}_{1-x}Eu^{3+}_{x}Ti^{4+}_{1-x/4}\square_{x/4}O_3$						
0.2	−62.8	−66.1	6.6°	−14.0	−16.2	7.0°
0.5	−175.7	−299.0	9.6°	−43.0	−100.2	10.4°
$Eu^{2+}_{1-x}Eu^{3+}_{2x/3}\square_{x/3}Ti^{4+}O_3$						
0.2	−12.1	−7.8	3.8°	−1.4	−0.7	3.0°
0.5	−9.2	−23.6	5.2°	−1.1	−19.6	5.0°
$Eu^{2+}_{1-x}Eu^{3+}_{x}Ti^{4+}_{1-x}Ti^{3+}_{x}O_3$						
0.2	−89.0	−104.6	7.3°	−19.1	−26.7	7.9°
0.5	−323.0	−514.3	11.0°	−82.5	−367.6	11.2°

The calculation results demonstrate that the phase with octahedron rotation $a^0a^0c^-$ and symmetry $I4/mcm$ is energetically favorable when the cubic structure is distorted in the eigenvectors of modes R_{25} and M_3 in the case of vacancy formation at the Ti^{4+} site and low Eu^{3+} concentrations. It is this phase that is experimentally detected in the $EuTiO_3$ compound, which undergoes a structural phase transition. Thus, the appearance of an antiferrodistortion instability was found to be related to an increase in the valence of the Eu ion and a decrease in the valence of the Ti ion, which agrees with the results in [10], where the antiferrodistortion transition in $EuTiO_3$ was assumed to be caused by the hybridization of the f electrons of Eu and the d electrons of Ti.

Table 5. Spontaneous polarization (μC/cm^2) in the polar phases of thin films of two thicknesses at various impurity Eu^{3+} concentrations

x	5 monolayers	17 monolayers
	P_x	P_x
0	51.6	20.7
$Eu^{2+}_{1-x}Eu^{3+}_{x}Ti^{4+}_{1-x/4}\square_{x/4}O_3$		
0.2	23.2	–
0.5	30.3	–
$Eu^{2+}_{1-x}Eu^{3+}_{2x/3}\square_{x/3}Ti^{4+}O_3$		
0.2	12.5	3.5
0.5	20.1	–
$Eu^{2+}_{1-x}Eu^{3+}_{x}Ti^{4+}_{1-x}Ti^{3+}_{x}O_3$		
0.2	26.8	8.1
0.5	32.7	11.3

Second, the lattice dynamics calculation of a thin $EuTiO_3$ film showed that its vibration spectrum has ferroelectric and antiferrodistortion instabilities. The ferroelectric $Pmm2$ phase is more favorable in the impurity-free compound, and the addition of an Eu^{3+} impurity leads to the energetically favorable antiferrodistortion deformation that causes the formation of the nonpolar $P4/mbm$ phase. However, the polar mode, the distortion in which gives polar phase Pm, remains unstable in the nonpolar phase in five-layer films. The polar phase appears in 17-layer films after the rotation of the oxygen octahedron only when Ti^{3+} substitutes for Ti^{4+} during the addition of an Eu^{3+} impurity.

ACKNOWLEDGMENTS

This work was supported by the Russian Foundation for Basic Research (project no. 12-02-00025-a) and the program Leading Scientific Schools of the President of the Russian Federation (project no. NSh-924.2014.2).

REFERENCES

1. T. Katsufuji and H. Takagi, Phys. Rev. B: Condens. Matter **64**, 054415 (2001).
2. T. R. McGuire, M. W. Shafer, R. J. Joenk, H. A. Alperin, and S. J. Pickart, J. Appl. Phys. **37**, 981 (1966).
3. C.-L. Chien, S. DeBenedetti, and F. D. S. Barros, Phys. Rev. B: Solid State **10**, 3913 (1974).
4. K. Z. Rushchanskii, N. A. Spaldin, and M. Lezaic, Phys. Rev. B: Condens. Matter **85**, 104109 (2012).

5. S. Kamba, D. Nuzhnyy, P. Vanek, M. Savinov, K. Knizek, Z. Shen, E. Santava, K. Maca, M. Sadowski, and J. Petzelt, Europhys. Lett. **80**, 27002 (2007).
6. G. J. Conduit and B. D. Simons, Phys. Rev. B: Condens. Matter **81**, 024102 (2010).
7. J. H. Lee, L. Fang, E. Vlahos, X. Ke, Y. W. Jung, L. F. Kourkoutis, J.-W. Kim, P. J. Ryan, T. Heeg, M. Roeckerath, V. Goian, M. Bernhagen, R. Uecker, P. C. Hammel, K. M. Rabe, S. Kamba, J. Schubert, J. W. Freeland, D. A. Muller, C. J. Fennie, P. Schiffer, V. Gopalan, E. Johnston-Halperin, and D. G. Schlom, Nature (London) **466**, 954 (2010).
8. C. J. Fennie and K. M. Rabe, Phys. Rev. Lett. **97**, 267602 (2006).
9. A. M. Glazer, Acta Crystallogr., Sect. B: Struct. Crystallogr. Cryst. Chem. **28**, 3384 (1972).
10. T. Birol and C. J. Fennie, Phys. Rev. B: Condens. Matter **88**, 094103 (2013).
11. A. Bussmann-Holder, J. Köhler, R. K. Kremer, and J. M. Law, Phys. Rev. B: Condens. Matter **83**, 212102 (2011).
12. M. Allieta, M. Scavini, L. J. Spalek, V. Scagnoli, H. C. Walker, C. Panagopoulos, S. S. Saxena, T. Katsufuji, and C. Mazzoli, Phys. Rev. B: Condens. Matter **85**, 184107 (2012).
13. J. Köhler, R. Dinnebier, and A. Bussmann-Holder, Phase Transitions **85**, 949 (2012).
14. J.-W. Kim, P. Thompson, S. Brown, P. S. Normile, J. A. Schlueter, A. Shkabko, A. Weidenkaff, and P. J. Ryan, Phys. Rev. Lett. **110**, 027201 (2013).
15. D. Bessas, K. Z. Rushchanskii, M. Kachlik, S. Disch, O. Gourdon, J. Bednarcik, K. Maca, I. Sergueev, S. Kamba, M. Ležaíc, and R. P. Hermann, Phys. Rev. B: Condens. Matter **88**, 144308 (2013).
16. V. Goian, S. Kamba, O. Pacherova, J. Drahokoupil, L. Palatinus, M. Dusek, J. Rohlicek, M. Savinov, F. Laufek, W. Schranz, A. Fuith, M. Kachl'ik, K. Maca, A. Shkabko, L. Sagarna, A. Weidenkaff, and A. A. Belik, Phys. Rev. B: Condens. Matter **86**, 054112 (2012).
17. J. H. Lee, X. Ke, N. J. Podraza, L. Fitting Kourkoutis, T. Heeg, M. Roeckerath, J. W. Freeland, C. J. Fennie, J. Schubert, D. A. Muller, P. Schiffer, and D. G. Schlom, Appl. Phys. Lett. **94**, 212509 (2009).
18. E. G. Maksimov, V. I. Zinenko, and N. G. Zamkova, Phys.—Usp. **47** (11), 1075 (2004).
19. M. Born and K. Huang, *Dynamical Theory of Crystal Lattices* (Clarendon, Oxford, 1954).
20. L. Bellaiche and D. Vanderbilt, Phys. Rev. B: Condens. Matter **61**, 7877 (2000).
21. A. R. Denton and N. W. Ashcroft, Phys. Rev. A: At., Mol., Opt. Phys. **43**, 3161 (1991).

Translated by K. Shakhlevich